Indoor Experiments on 4-by-2 Multi-user MIMO Employing Various Transmitter Antenna Arrangements in LTE-Advanced Downlink

Yuichi Kakishima[†], Teruo Kawamura[†], Yoshihisa Kishiyama[†], Hidekazu Taoka[‡], and Hidehiro Andoh[†]

[†]Radio Access Network Development Department
NTT DOCOMO, INC.
3-5 Hikari-no-oka, Yokosuka-shi, Kanagawa-ken 239-8536 Japan

[‡]DOCOMO Communications Laboratories Europe GmbH
Landsberger Strasse 312, 80687, Munich, Germany

Abstract – **This paper presents indoor experimental results on the achievable throughput for 4-by-2 multi-user (MU)-MIMO using 2 mobile stations (MSs) and carrier aggregation with 5 component carriers (90-MHz bandwidth) considering various transmitter antenna arrangements in the LTE-Advanced downlink. Under two centralized and two distributed antenna arrangement (CAAs and DAAs) conditions, the throughput performance is evaluated using the implemented LTE-Advanced transceiver, where extended channel state information (CSI) feedback based on eigenvalue decomposition (EVD) is implemented for MU-MIMO operation. The experimental results show that the peak throughput of greater than 1 Gbps is achieved for the CAAs in an indoor environment. The results also showed that although the MS moving speed strongly influences the throughput for Rank-4 MU-MIMO, MU-MIMO is robust against the antenna separation, i.e., fading correlation. Furthermore, we confirm that, in the DAAs, although the peak throughput of 1 Gbps is not observed, the throughput of approximately 700 to 950 Mbps is achieved.**

Keywords – LTE-Advanced; multi-user MIMO; antenna arrangement; indoor experiment

I. INTRODUCTION

The 3rd Generation Partnership Project (3GPP) finalized the radio interface specifications for the next generation mobile communication system called Long-Term Evolution (LTE) as Release 8 [1],[2]. LTE provides full IP packet-based radio access with low latency and adopts intra-cell orthogonal multiple access schemes, i.e., orthogonal frequency division multiple access (OFDMA) and single-carrier frequency division multiple access (SC-FDMA), in the downlink and uplink, respectively. In Japan, NTT DOCOMO launched a commercial LTE service in December 2010 under the new service brand of "Xi" (crossy) [3]. Among 3GPP standardization activities, there have been efforts towards establishing the enhanced LTE radio interface called LTE-Advanced (LTE Release 10 and beyond) and specifications for LTE Release 10 were finalized [4],[5]. In LTE-Advanced, it is necessary to support a wider bandwidth than that in LTE Release 8, i.e., 20 MHz, to satisfy the high level requirements corresponding to the target peak data rate of greater than 1 Gbps. Toward this end, LTE-Advanced supports carrier aggregation (CA) up to 100 MHz by aggregating multiple component carriers (CCs) with backward compatibility to LTE Releases 8/9. In addition, to satisfy the requirements for further improvement in terms of spectrum efficiency, enhanced multiple-input multiple-output (MIMO) techniques such as higher-order MIMO multiplexing and multi-user (MU)-MIMO are supported.

Enhanced MU-MIMO in the downlink is an essential technique to satisfy the International Telecommunication Union Radio-communication sector (ITU-R) requirements for cell spectrum efficiency and cell-edge spectrum efficiency in macro-cellular and base coverage urban environments [6]. In LTE-Advanced, two types of reference signals (RSs) are newly defined: the RS used for channel state information (CSI) estimation, i.e., the CSI-RS, and the RS used for data demodulation, i.e., the DM-RS. These RSs enable enhanced MU-MIMO with inter-user interference control in the LTE-Advanced downlink. The higher-rank transmission using MU-MIMO is beneficial because that using SU-MIMO is often limited by the number of antennas for a set of user equipment (UE). In [6], 4-by-2 MU-MIMO is assumed as one of the antenna configurations. When the base station (BS) spatially multiplexes the maximum of four data streams, which exceeds the number of receiver antennas per UE, very accurate CSI feedback is required so that the BS can generate precoding weights to reduce the mutual interference between the transmitted data streams of spatially multiplexed UEs [7]-[9]. Therefore, in our experimental equipment, we implement extended CSI feedback based on eigenvalue decomposition (EVD) with respect to each subband (SB) to evaluate the potential performance of LTE-Advanced MU-MIMO although it is not yet standardized as an LTE-Advanced specification.

In [10], we reported that in laboratory experiments using a fading simulator, the downlink throughput of 1 Gbps is achieved by applying 4-by-2 Rank-4 MU-MIMO to 2 mobile stations (MSs) using CA with 5 CCs (90-MHz bandwidth) based on experimental equipment employing the LTE-Advanced radio interface, i.e., the CSI-RS and DM-RS. The performance of MU-MIMO highly depends on the propagation channel conditions such as the fading correlation, i.e., antenna configurations. Therefore, this paper investigates the performance of MU-MIMO considering various BS-antenna arrangements using the implemented LTE-Advanced transceiver in a real indoor propagation environment. More specifically, we show a peak throughput that exceeds 1 Gbps for 4-by-2 Rank-4 MU-MIMO using adaptive modulation and coding (AMC) and hybrid automatic repeat request (HARQ) based on indoor experiments that were conducted at the NTT DOCOMO R&D Center in Yokosuka, Japan. Furthermore, we clarify the influence of the MS moving speed, antenna separation (fading correlation), and transmitter antenna arrangement on the achievable throughput of MU-MIMO. The rest of the paper is organized as follows. In Section II, the MU-MIMO scheme implemented for experimental evaluation is outlined. After describing the configuration of the implemented transceiver in Section III, the measurement environment and indoor experimental results are presented in Section IV. Finally, Section V presents our conclusions.

II. MU-MIMO SCHEME FOR EXPERIMENTAL EVALUATIONS

A. Time/Frequency Granularity for MU-MIMO Operation

In the paper, downlink MU-MIMO with a single BS and two MSs is evaluated in indoor experiments, where the number of BS transmitter antennas, N_{TX}, is four, the number of receiver antennas for each MS,

978-1-4673-1881-5/12/$31.00 ©2012 IEEE

N_{RX}, is two, and the maximum number of data streams per MS is two. Figure 1 shows the RS mapping for the implemented LTE-Advanced transceiver. In the frequency domain, each CC consists of multiple SBs, which represent the unit of CSI feedback. Each SB has the bandwidth of F_{CSI} and consists of multiple resource blocks (RBs), each of which contains 12 subcarriers. In the time domain, the subframe duration, i.e., transmission time interval (TTI), is 1 msec, which contains 14 OFDM symbols. The RS used for CSI estimation, i.e., the CSI-RS, for each transmitter antenna is periodically multiplexed with the time duration of several TTIs, T_{CSI}, and mapped every six subcarriers, where frequency division multiplexing (FDM) is used to multiplex the CSI-RSs among four transmitter antennas. Thus, the precoding weights for MU-MIMO transmission are updated with the same periodicity as that for the CSI-RS with the additional control delay of 10 msec. The RS used for demodulation of the data stream, i.e., the DM-RS, which is precoded in the same manner as each data stream, is multiplexed with the insertion density of 12 resource elements (REs) per RB per data stream and within each subframe. For Rank-4 MU-MIMO, code division multiplexing (CDM) is used to multiplex the DM-RSs between two data streams for the same MS, and FDM is used between two MSs as shown in the Fig. 1. For Rank-2 MU-MIMO, CDM is applied to multiplex the DM-RSs between two MSs.

B. CSI Feedback Scheme

The MS calculates the CSI as feedback information and notifies the BS. The MS calculates the eigenvalues and the eigenvectors of the covariance matrix of the measured channel, and the received signal-to-interference plus noise power ratio (SINR) for each SB. At the u-th MS (u = 1 or 2), the downlink channel matrix ($N_{RX} \times N_{TX}$) on the k-th subcarrier, $\mathbf{H}_u(k)$, is estimated using the received CSI-RS, which is denoted as $\hat{\mathbf{H}}_u(k)$. Then, the covariance matrix of $\hat{\mathbf{H}}_u(k)$ for each SB, $\overline{\mathbf{R}}_u$, is calculated by averaging $\hat{\mathbf{H}}_u^{\mathrm{H}}(k)\hat{\mathbf{H}}_u(k)/S_u$ within the SB in the frequency and time domains, where S_u is the average received CSI-RS power for the normalization to remove the effect of path loss and shadowing. Below, the calculation of the CSI feedback within a SB is presented. We omit the index of the SB for simplicity. By applying the Jacobi EVD [11] to the channel covariance matrix as $\overline{\mathbf{R}}_u = \mathbf{U}_u \mathbf{D}_u^2 \mathbf{U}_u^{\mathrm{H}}$, eigenvalues $\mathbf{D}_u^2 = \mathrm{diag}\{\lambda_{u,1}^2, \lambda_{u,2}^2, \lambda_{u,3}^2, \lambda_{u,4}^2\}$ for $\lambda_{u,1}^2 \geq \lambda_{u,2}^2 \geq \lambda_{u,3}^2 \geq \lambda_{u,4}^2$, and the corresponding eigenvectors, $\mathbf{U}_u = (\mathbf{u}_{u,1}\ \mathbf{u}_{u,2}\ \mathbf{u}_{u,3}\ \mathbf{u}_{u,4})$, are derived. The N_{stream} highest eigenvalues and the corresponding eigenvectors are selected for the CSI feedback, where N_{stream} represents the number of data streams per MS. Furthermore, the SINR for the i-th data stream (i = 1 or 2) of the u-th MS is calculated as $\gamma_{u,i} = \lambda_{u,i}^2 S_u / \sigma_u^2$, where σ_u^2 is the average noise power estimated using the received CSI-RS.

Each complex eigenvector component is quantized by 13 bits, which comprise 7 bits for phase and 6 bits for amplitude, using star-type mapping for each transmitter antenna and data stream. The eigenvalue and SINR for each data stream are quantized by 5 and 7 bits, respectively. Therefore, the total number of CSI feedback bits per MS becomes $N_{CC} \times N_{SB} \times N_{stream} \times 64$ bits, where N_{CC} and N_{SB} represent the number of CCs and SBs per CC, respectively.

C. Precoding Weight Generation Scheme

At the BS transmitter, the precoding weights for downlink MU-MIMO are calculated based on the CSI transmitted from the two MSs in the uplink. Here, the composite channel matrix for each SB of the u-th MS is defined as $\mathbf{G}_u = (\hat{\lambda}_{u,1}\hat{\mathbf{u}}_{u,1}\ \ \hat{\lambda}_{u,2}\hat{\mathbf{u}}_{u,2})^{\mathrm{H}}$ for Rank-4 MU-MIMO, where $\hat{\lambda}_{u,i}$ and $\hat{\mathbf{u}}_{u,i}$ are the quantized eigenvalue and the corresponding eigenvector, respectively. The precoding weight matrix for each SB, $\mathbf{V}$, is defined as $\mathbf{V} = (\mathbf{v}_{1,1}\ \mathbf{v}_{1,2}\ \mathbf{v}_{2,1}\ \mathbf{v}_{2,2})$, where $\mathbf{v}_{u,i}$ is the $N_{TX} \times 1$ precoding weight vector. In this paper, $\mathbf{V}$ is calculated based on the MMSE criteria as

$$\mathbf{V} = \mathbf{G}^{\mathrm{H}}(\mathbf{G}\mathbf{G}^{\mathrm{H}} + \mathbf{E})^{-1}, \tag{1}$$

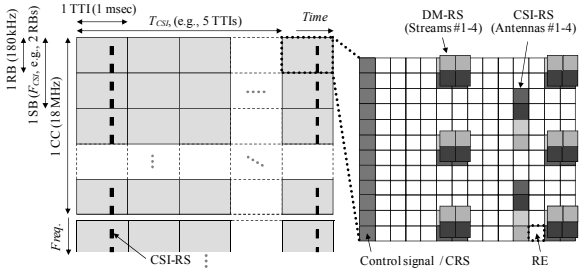

Figure 1. RS mapping for implemented LTE-Advanced transceiver (Rank-4 MU-MIMO)

where $\mathbf{G} = \left(\mathbf{G}_1^{\mathrm{T}}\ \mathbf{G}_2^{\mathrm{T}}\right)^{\mathrm{T}}$, $\mathbf{E} = \mathrm{diag}\{\hat{\gamma}_{1,1}^{-1}\ \hat{\gamma}_{1,2}^{-1}\ \hat{\gamma}_{2,1}^{-1}\ \hat{\gamma}_{2,2}^{-1}\}$, and $\hat{\gamma}_{u,i}$ is the quantized SINR reported by the MSs. By using the normalized precoding weights, $\overline{\mathbf{v}}_{u,i} = \mathbf{v}_{u,i} / \|\mathbf{v}_{u,i}\|$, the transmission signal vector on the k-th subcarrier for $N_{TX} = 4$ is represented as

$$\mathbf{s}(k) = \sum_{u=1}^{2}\sum_{i=1}^{2} \overline{\mathbf{v}}_{u,i} d_{u,i}(k), \tag{2}$$

where $d_{u,i}(k)$ represents the modulated data sequence. Furthermore, $\overline{\mathbf{v}}_{u,i}$ is constant within the SB but varies among the SBs.

III. Configuration of Implemented LTE-Advanced Transceiver

The major radio link parameters and the configuration of the implemented transceiver are given in Table I and Fig. 2, respectively. The transmission bandwidth and the number of subcarriers of the OFDM signal in the downlink are 90 MHz and 6000, respectively (thus, the subcarrier separation is 15 kHz). We employ CA using N_{CC} = 5 (each CC has an 18-MHz transmission bandwidth, which is supported in LTE Release 8) with contiguous spectrum allocation. In the paper, F_{CSI} and T_{CSI} for MU-MIMO operation are set to 900 kHz (= 5 RBs, N_{SB} becomes 20) and 5 msec, respectively. In the BS transmitter, the information binary data sequence for each data stream, CC, and MS is independently turbo encoded with the coding rate of R and modulated. After multiplexing the DM-RS, the precoding weights for MU-MIMO are multiplied to the data stream and DM-RS. Then, the CSI-RS for each transmitter antenna is multiplexed and the resultant signal sequence is converted into an OFDM symbol with the duration of 66.67 μsec using an 8192-point inverse fast Fourier transform (IFFT) followed by the addition of a cyclic prefix (CP) of 4.69 μsec. After conversion into baseband in-phase (I) and quadrature (Q) components using digital-to-analog (D/A) converters, quadrature modulation is performed. Finally, the intermediate frequency (IF) modulated signal is up-converted into the radio frequency (RF) signal and amplified by the power amplifier, where the center carrier frequency is 3.92625 GHz.

At each MS receiver, we apply two-branch antenna diversity reception. The frequency down-converted IF signal is first linearly amplified by an automatic gain control (AGC) amplifier with the dynamic range of approximately 50 dB. The received signal is converted into baseband I and Q components by a quadrature detector. The I and Q signals are converted into a digital format using 14-bit analog-to-digital (A/D) converters. After the CP is removed, the OFDM signal is de-multiplexed into the data signal, CSI-RS, and DM-RS using an 8192-point FFT. After an interference whitening filter is applied in order to randomize the interfering data streams that are transmitted to the other MS [12],[13], the maximum likelihood detection (MLD) is performed to separate the two data streams that are transmitted to its own MS. Channel estimation for interference whitening and signal detection is performed for each SB using the DM-RS. Finally, the sequence of likelihood values after MLD is turbo decoded using the Max-Log-MAP algorithm with six iterations to recover the transmitted binary data. Furthermore, CSI is estimated using the received CSI-RS and fed back to the BS via the uplink shared channel.

TABLE I. MAJOR RADIO LINK PARAMETERS

Carrier frequency		3.92625 GHz
OFDM signal bandwidth		90 MHz (18 MHz x 5 CCs)
Number of subcarriers		6000 (1200 x 5 CCs)
Subcarrier separation		15 kHz
Subframe length		1 msec (14 OFDM symbols)
OFDM symbol duration	Effective data	66.67 μsec
	Cyclic prefix	4.69 μsec
Number of antennas		BS: 4, MS: 2
Number of MSs		2
Channel coding / decoding		Turbo coding (coding rate: R) / Max-Log-MAP decoding (6 iterations)
SB size (F_{CSI})		900 kHz (5 RBs)
CSI-RS transmission period (T_{CSI})		5 msec
Control delay for precoding		10 msec
Control delay for AMC		10 msec
HARQ	Packet combining	IR
	Max. number of transmissions	3
	Round trip delay	8 msec

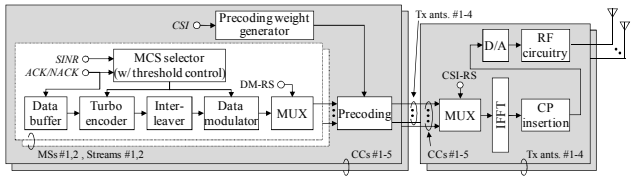

(a) BS transmitter

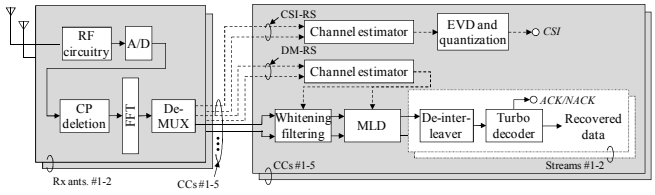

(b) MS receiver

Figure 2. Configuration of implemented LTE-Advanced transceiver

Table II summarizes the set of twelve modulation and coding scheme (MCS) sets used for AMC in the experiments. The AMC is performed according to the instantaneous received SINR reported by the MS. In order to compensate for the fluctuation in the measured SINR values due to the mutual interference between spatially multiplexed MSs, the SINR threshold for MCS selection is adaptively adjusted using outer-loop control based on acknowledgement (ACK) / negative ACK (NACK) feedback signaling from the MS [14]. The control delay of AMC is 10 msec. We use incremental redundancy (IR) for HARQ with packet combining and the round trip delay is 8 msec. The maximum number of transmissions for HARQ is set to three.

IV. INDOOR EXPERIMENTAL RESULTS

A. Measurement Environment

We investigate the MU-MIMO performance in a conference room at the NTT DOCOMO R&D Center, which is representative of an indoor office environment. The dimensions, i.e., width, depth, and height, of the room are 18.4 m × 12.2 m × 3.8 m, and 40 office desks with the height of 70 cm and 80 office chairs are arranged. Figure 3 shows BS-antenna and MS arrangements, and the measurement course. For the centralized antenna arrangements (CAAs), the BS antennas are located at the center of the room, and four dipole antennas are linearly arranged with the adjacent antenna separation, Δ_{BS}, as a parameter. The antenna array direction in CAAs #1 and #2 is perpendicular and parallel to the measurement course, respectively. For distributed antenna arrangement (DAA) #1, the four BS antennas are arranged near each vertex of a rectangle with the size of 6.0 m × 9.6 m, and for DAA #2, the rectangle size is set to 7.6 cm (corresponds to one times the carrier frequency, i.e., 1.0λ) × 9.6 m.

TABLE II. MCS SETS FOR AMC

Index	Modulation	Coding Rate	Index	Modulation	Coding Rate
1	QPSK	0.39	7	64QAM	0.56
2		0.47	8		0.65
3	16QAM	0.38	9		0.73
4		0.49	10		0.78
5		0.58	11		0.81
6	64QAM	0.47	12		0.96

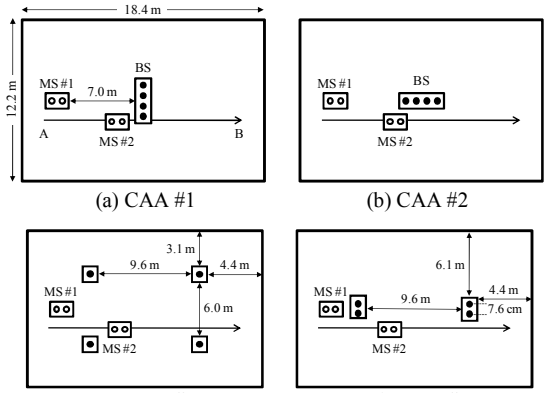

Figure 3. BS-antenna and MS arrangements

MS #1 is static (v_1 = 0 km/h) and is placed at one end of the room around Point A. MS #2 travels along the course with the entire length of approximately 14 m from Point A to Point B with the moving speed, v_2, as a parameter. Two MS antennas are arranged with the adjacent antenna separation, Δ_{MS}, as a parameter. The BS and MS antennas are dipole antennas with omni-directional beam patterns in azimuth with the gain of 2 dBi and placed at the height of 2.4 m and 1.4 m from the floor, respectively. In the experiments, the BS transmission power is set to 20 dBm (=100 mW). Over the entire course, the BS antennas are in direct view from the MS antennas, i.e., line-of-sight (LOS) conditions. The root mean squared (r.m.s.) delay spread of the measurement course, which is calculated based on the received CSI-RSs, is approximately 0.05 μsec.

B. Throughput Performance in CAA #1

First, we present experimental results on the throughput performance of 4-by-2 MU-MIMO in CAA #1. Figure 4 shows examples of the time variation in the estimated SINR, the MCS selection probability, and the measured throughput for each data stream of MS #2 when Rank-4 MU-MIMO is applied. In this evaluation, we assume Δ_{BS} = Δ_{MS} = 7.6 cm (1.0λ) and v_2 = 1 km/h. The SINR and the throughput are averaged over the duration of 200 msec and the MCS selection probability is calculated in 1-sec intervals. Figure 4 shows that the received SINR for each data stream fluctuates over time in the range of approximately 8 dB, and the average received SINR for streams #1 and #2 become approximately 25 and 17 dB, respectively. The difference in the received SINR between data streams is due to the EVD-based precoding weight generation, i.e., the eigenvalue of the first stream is greater than that for the second stream. This figure also shows that the received SINR for the stream #1 is degraded around the center of the measurement course. The reason for this is considered to be that the antenna gain is not sufficiently obtained when MS #2 passes just below the BS antennas. From the results on the MCS selection probability, we find that the appropriate MCS set is selected according to the measured SINR, and then the MCS using 64QAM and that using 16QAM are chosen at the rate of approximately 99% and 85% for data streams #1 and #2, respectively. As a result, in the region where MCS combinations of {64QAM, R = 0.78} for stream #1 and {16QAM, R = 0.58} for stream #2 are mainly selected, the total throughput of greater than 400 Mbps is achieved.

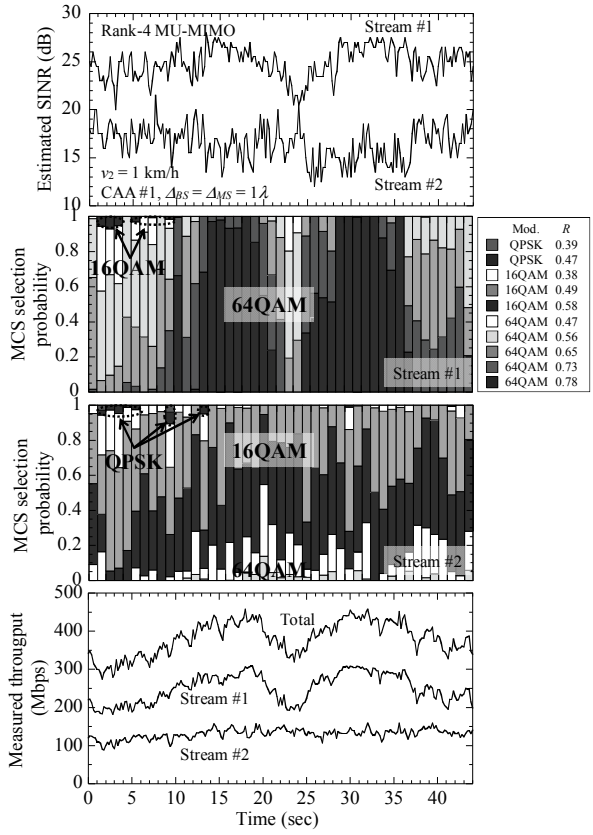

Figure 4. Examples of time variation in downlink performances for Rank-4 MU-MIMO (MS #2)

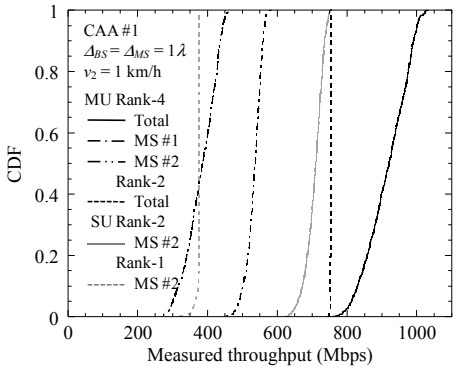

Figure 5. CDF of throughput performance

Figure 5 shows the cumulative distribution function (CDF) of the measured throughput for each MS and their sum total when Rank-4 MU-MIMO is applied. The evaluation conditions are the same as those in Fig. 4. In Fig. 5, we also plot the throughput performance for 4-by-2 Rank-2 MU-MIMO and 4-by-2 Rank-2/1 SU-MIMO for comparison. In the SU-MIMO transmission, EVD-based precoding is applied, which is identical to that for MU-MIMO. Figure 5 shows that the throughput for Rank-2 SU-MIMO is superior to that of Rank-4 MU-MIMO for each MS because there is no mutual interference between the spatially multiplexed MSs. However, the throughput of 450 to 570 Mbps for MS #1 for Rank-4 MU-MIMO, which is statically located at one end of the room, is observed and consequently, the total throughput, which is defined as the sum total throughput for each MS, is greater than 1 Gbps at the location probability of approximately 5%. As a result, we clearly find that the throughput for Rank-4 MU-MIMO is greater than that for Rank-2 SU-MIMO over the entire measurement course and we confirm the superiority of MU-MIMO compared to SU-MIMO in an indoor environment. Focusing on Rank-2 transmission, based on Fig. 5, we

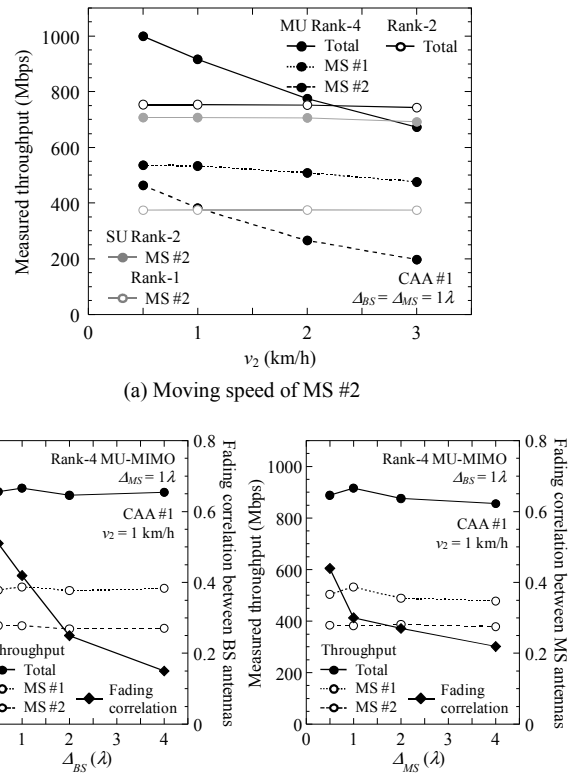

(a) Moving speed of MS #2

(b) BS or MS antenna separation

Figure 6. Impact of moving speed and antenna separation on throughput for Rank-4 MU-MIMO

also find that Rank-2 MU-MIMO is superior to Rank-2 SU-MIMO over the entire measurement course although the same peak throughput of approximately 750 Mbps is achieved. This is because the eigenmode transmission with the highest eigenvalue for each MS for Rank-2 MU-MIMO sufficiently suppresses the mutual interference in this environment, although the eigenmode transmission with the first and second eigenvalues is employed for 2 data stream transmission in Rank-2 SU-MIMO.

Next, we present the influence of the MS moving speed and the antenna separation, i.e., fading correlation, for the BS and MS on the achievable throughput for MU-MIMO. Figure 6(a) shows the throughput performance for Rank-4 MU-MIMO averaged over the entire measurement course when v_2 is parameterized as 0.5, 1, 2, and 3 km/h. In the evaluation, we assume $\Delta_{BS} = \Delta_{MS}$ = 7.6 cm (1.0λ). In Fig. 6(a), we also plot the throughput performance for Rank-2 MU-MIMO and Rank-2/1 SU-MIMO for comparison. The figure shows that the throughput for MS #2 for Rank-4 MU-MIMO is largely degraded according to the increase in the v_2 value due to the degradation in the tracking ability for CSI feedback for MS #2 compared to the other cases. Here, we also find that the throughput of MS #1 for Rank-4 MU-MIMO, which is statically located at one end of the room, is marginally degraded according to the increase in v_2. The reason for this is considered to be the fluctuation in the propagation channel between the BS and MS #1 and the mutual interference due to the movement of MS #2. On the other hand, it is clear in Fig. 6(a) that the throughput performance for Rank-2 MU-MIMO (Rank-2 SU-MIMO) is robust against v_2 assuming a walking speed and that the throughput of approximately 750 (700) Mbps is constantly achieved. Figure 6(b) shows the throughput performance for Rank-4 MU-MIMO averaged over the entire measurement course when Δ_{BS} and Δ_{MS} are parameterized as 3.8, 7.6, 15.3, and 30.6 cm, which correspond to 0.5λ, 1.0λ, 2.0λ, and 4.0λ, respectively. In the evaluation, we assume that when Δ_{BS} (Δ_{MS}) is parameterized, Δ_{MS} (Δ_{BS}) is set to 7.6 cm (1.0λ), and v_2 = 1 km/h. In the figure, we also plot the fading correlation value between adjacent BS or MS

antennas for each antenna separation condition, which is calculated based on the channel response estimated by using the received CSI-RSs. Figure shows that almost the same throughput of approximately 900 Mbps is achieved irrespective of the Δ_{BS} and Δ_{MS} values. The reason for this is considered to be that the fading correlation between the adjacent antennas becomes relatively low, e.g., approximately 0.5, even when Δ_{BS} or Δ_{MS} is set to 3.8 cm (0.5λ), since the reflected waves arrive from every direction in an indoor environment.

C. Influence of Transmitter Antenna Arrangements on Throughput

Finally, we present the influence of the transmitter antenna arrangements as shown in Fig. 3 on the achievable throughput for 4-by-2 MU-MIMO. In this evaluation, we assume $\Delta_{BS} = \Delta_{MS} = 7.6$ cm (1.0λ) and $v_2 = 1$ km/h. Figure 7(a) shows the CDF of the measured received signal strength indicator (RSSI) of MS #2 for each BS-antenna arrangement. The RSSI is averaged over the duration of 200 msec. Figure 7(a) shows that CAAs have a RSSI distribution within the range of approximately −52 to −39 dBm while the range of the distribution for DAAs is −49 to −42 dBm. The fluctuation for the DAAs is smaller than that for the CAAs. Based on these results, we find that the DAAs cover a wider area with a certain received signal level compared to the CAAs. Figure 7(b) shows the CDF of the eigenvalue ratio of MS #2, which is defined as the ratio of the second eigenvalue to the first eigenvalue ($\lambda_{u,2}^2 / \lambda_{u,1}^2$). Figure 7(b) shows that the eigenvalue ratios for CAA #1 and DAA #2 are greater than those for CAA #2 and DAA #1, respectively. The calculated fading correlation values between the nearest BS antennas for CAAs #1 and #2 and DAAs #1 and #2 are 0.42, 0.20, 0.10, and 0.40, respectively. Considering the results, we find that the lower fading correlation contributes to lower eigenvalue ratios for CAA #2 and DAA #1.

Figure 8 shows the throughput comparison among transmitter antenna arrangements for Rank-4 MU-MIMO. In Fig. 8, we plot the measured throughput for each MS and their sum total. The throughput is averaged over the duration of 200 msec. Figure shows that although the average RSSI values of MS #2 for all antenna arrangements are comparable levels as shown in Fig. 7(a), the throughput performances of MS #2 for CAAs are obviously better than those for DAAs. This is because the angler difference between MSs viewed from BS antennas in CAAs becomes large compared to DAAs, it is believed that the mutual interference between MSs can be effectively suppressed by applying the beam forming. Consequently, the total throughput of greater than 1 Gbps is achieved at the location probability of approximately 5% using CAA #1 or #2. The figure also shows that the throughput performance of MS #2 for DAA #2 is slightly larger than that for DAA #1, which is in the same manner as the performance of RSSI. As a result, although the peak throughput of 1 Gbps is not observed in DAAs since the large RSSI such as greater than approximately −43 dBm is not obtained as shown in Fig. 7(a), the throughput of approximately 700 to 950 Mbps is achieved in an indoor environment.

V. CONCLUSION

This paper presented indoor experimental results on the achievable throughput for 4-by-2 MU-MIMO using 2 MSs and CA with 5 CCs (90-MHz bandwidth) considering various transmitter antenna arrangements in the LTE-Advanced downlink. For two CAAs and two DAAs, the throughput performance was evaluated using the implemented LTE-Advanced transceiver, where extended CSI feedback based on EVD was implemented for MU-MIMO operation. The experimental results showed that the peak throughput of greater than 1 Gbps is achieved for the CAAs in an indoor environment. The results also showed that although the MS moving speed strongly influences the throughput for Rank-4 MU-MIMO, MU-MIMO is robust against the antenna separation, i.e., fading correlation. Furthermore, we confirmed that, in the DAAs, although the peak throughput of 1 Gbps is not observed, the throughput of approximately 700 to 950 Mbps is achieved.

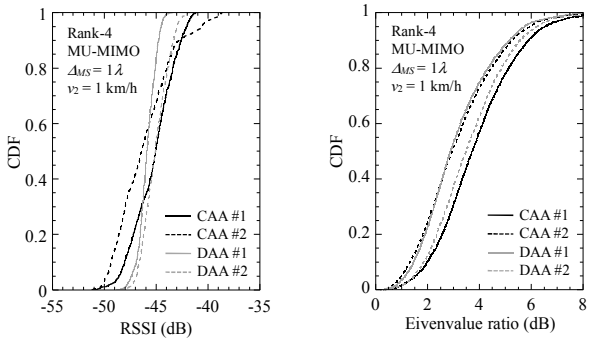

(a) CDF of RSSI (b) CDF of eigenvalue ratio

Figure 7. RSSI and eigenvalue ratio of each transmitter antenna arrangement for Rank-4 MU-MIMO (MS #2)

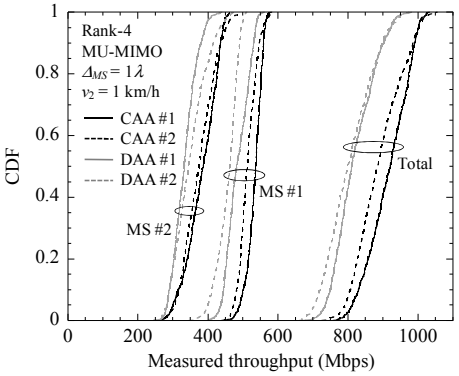

Figure 8. Throughput comparison among transmitter antenna arrangements for Rank-4 MU-MIMO

REFERENCES

[1] 3GPP, TS 36.300 (V8.12.0), "Evolved Universal Terrestrial Radio Access (E-UTRA) and Evolved Universal Terrestrial Radio Access Network (E-UTRAN); Overall description; Stage 2 (Release 8)," Apr. 2010.

[2] M. Tanno, Y. Kishiyama, N. Miki, K. Higuchi, and M. Sawahashi, "Evolved UTRA - physical layer overview," Proc. IEEE SPAWC 2007, June 2007.

[3] http://www.nttdocomo.com/pr/2010/001494.html

[4] 3GPP, TS 36.201 (V10.0.0), "Evolved Universal Terrestrial Radio Access (E-UTRA); LTE physical layer; General description (Release 10)," Dec. 2010.

[5] E. Dahlman, S. Parkvall, and J. Sköld, "4G – LTE/LTE-Advanced for Mobile Broadband," Academic Press, 2011.

[6] 3GPP, TR 36.912 (V10.0.0), "Feasibility Study for Further Advancements for E-UTRA (LTE-Advanced) (Release 10)," Mar. 2011.

[7] D. Love, R. Heath, V. Lau, D. Gesbert, B. Rao, and M. Andrews, "An overview of limited feedback in wireless communication systems," IEEE J. Sel. Areas Commun., vol. 26, no. 8, pp. 1341-1365, Oct. 2008.

[8] M. Trivellato, F. Boccardi, and H. Huang, "On transceiver design and channel quantization for downlink multiuser MIMO systems with limited feedback," IEEE J. Sel. Areas Commun., vol. 26, no. 8, pp. 1494-1504, Oct. 2008.

[9] C. Guthy, W. Utschick, and G. Dietl, "Finite rate feedback schemes for the MIMO OFDM broadcast channel," International ITG workshop on smart antennas - WSA 2008, Feb. 2008.

[10] Y. Kakishima, T. Kawamura, Y. Kishiyama, H. Taoka, and T. Nakamura, "Experimental evaluations on carrier aggregation and multi-user MIMO associated with EVD-based CSI feedback for LTE-Advanced downlink," Proc. IEEE ISWCS'11, Nov. 2011.

[11] B. T. Smith, J. M. Boyle, and J. J. Dongarra, Matrix Eigensystem Routines – EISPACK Guide, 2nd ed., vol. 6 of lecture notes in computer science, Springer, 1988.

[12] D. Tse and P. Viswanath, Fundamentals of Wireless Communication, Cambridge University Press, 2005.

[13] S. Shim, J. S. Kwak, R. Heath, and J. Andrews, "Block diagonalization for multi-user MIMO with other-cell interference," IEEE Trans. on Wireless Commun., vol. 7, no. 7, pp. 2671-2681, July 2008.

[14] J. Lee, R. Arnott, K. Hamabe, and N. Takano, "Adaptive modulation switching level control in high speed downlink packet access transmission," 3G Mobile Communication Technologies, pp. 156-159, May 2002.